# Supplementary Materials for

## Mechanically-induced remodeling of the cell surface generates actin-rich protrusions resembling tunneling nanotubes

Juliana Soares *et al.*

*Corresponding author. Email: bpontes@icb.ufrj.br

**This PDF file includes:**

Supplementary Text
Figs. S1 to S4
Table S1
Movies S1 to S14

**Other Supplementary Materials for this manuscript include the following:**

Movies S1 to S14

**Supplementary Text**

Determination of $A^2$

The parameter $A^2$ was obtained using *Mathematica* (Wolfram Research Inc., USA). The raw force time series $F_{\text{raw}}(t)$ consisted of $2n = 600$ points, acquired at a sampling frequency of $f_{\text{aq}} = 10$ fps, corresponding to a total duration of $T = 1$ minute and a time step of $\Delta t = T/2n = 0.1$ s. Outliers were removed using the function $DeleteAnomalies[\dots]$. The power spectral density was calculated after the average subtraction $F(t) = F_{\text{raw}}(t) - Mean[F_{\text{raw}}(t)]$, by using the functions *Fourier* $[\dots]$ and $Abs[\dots]$:

$$PSD_F(\nu) = 2 * \Delta t * Abs\left[Fourier[F(t)]\right]^2, \quad (1)$$

where the discrete frequency $\nu = \frac{i}{T}$ with $i = 1,2,3, \dots, n$is defined in the interval $\left[1/T, 1/2\Delta t\right]$. In this frequency range, by the Wiener–Khinchin theorem, the normalization factor corresponds to the force variance and can be determined as:

$$\langle F^2 \rangle = \frac{Total[\, PSD_F(\nu)\,]}{2\ \Delta t\ n}. \quad (2)$$

Those definitions lead to the discrete frequency increment $\Delta\nu = \frac{1}{2\ \Delta t\ n}$, that allows to determine $A^2$ as:

$$A^2 = \frac{1}{\langle F^2 \rangle} \sum_{\nu=0}^{0.5} PSD_F(\nu)\Delta\nu. \quad (3)$$

**Figs. S1 to S4**

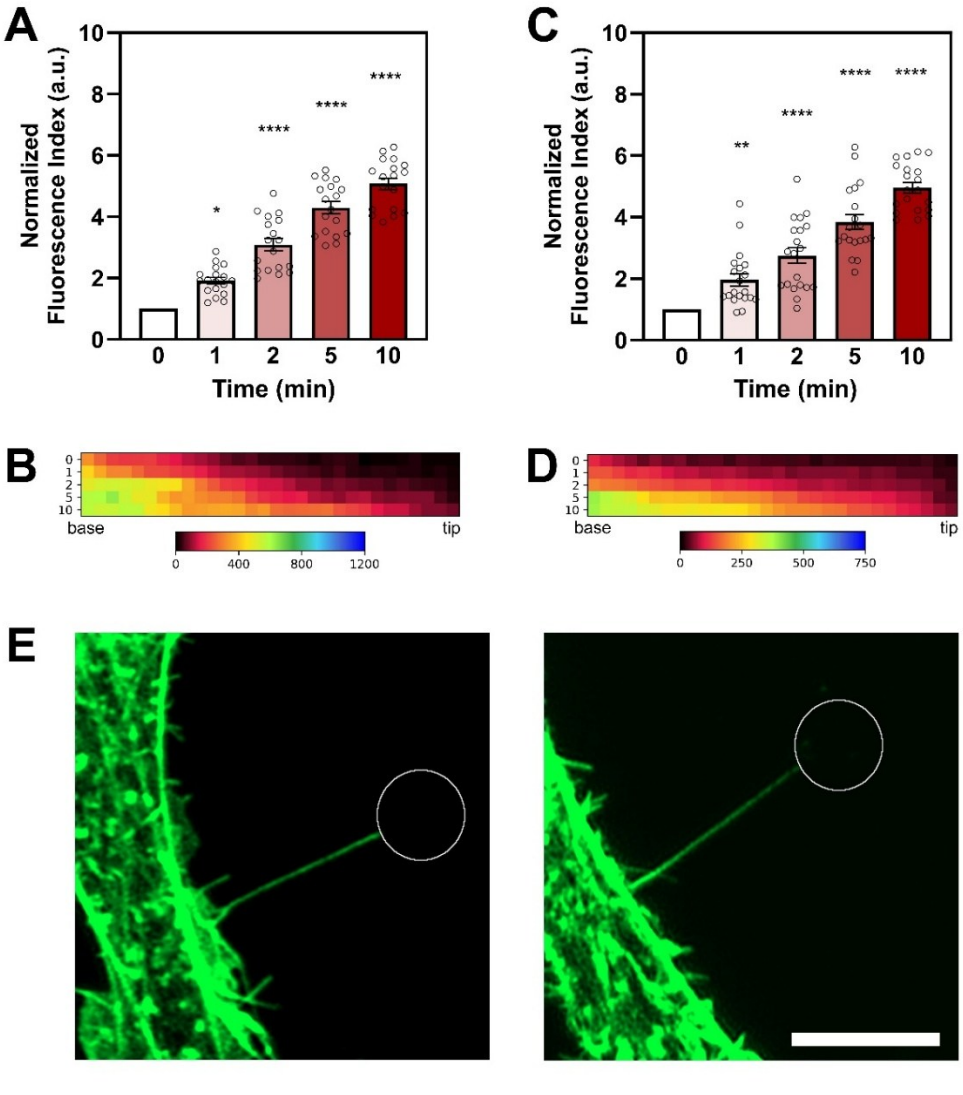


**Fig. S1. F-actin recruitment within tethers using F-tractin, different extraction velocity, and phalloidin staining.** (A) Average F-actin fluorescence intensity over time measured with Lifeact-mEGFP (normalized to 0 min) in tethers extracted at 100 μm/s. (B) Heatmap showing Lifeact-mEGFP intensity distribution along the entire tether length at 0, 1, 2, 5, and 10 min ($n \geq 15$). Tether was divided into 30 bins; base = near cell, tip = near bead. (C) Average F-actin fluorescence intensity over time measured with F-tractin-EGFP (normalized to 0 min) in tethers extracted at 1 μm/s. (D) Heatmap showing F-tractin-EGFP intensity distribution along the tether length at 0, 1, 2, 5, and 10 min ($n \geq 15$). (E) Representative confocal images of phalloidin-FITC staining confirming the presence of F-actin in tethers, consistent with and following previous report (1). Error bars in A and B represent standard errors. Scale bar in E: 5μm. Statistical significance: * $p \leq 0.05$; ** $p < 0.01$; **** $p < 0.0001$.

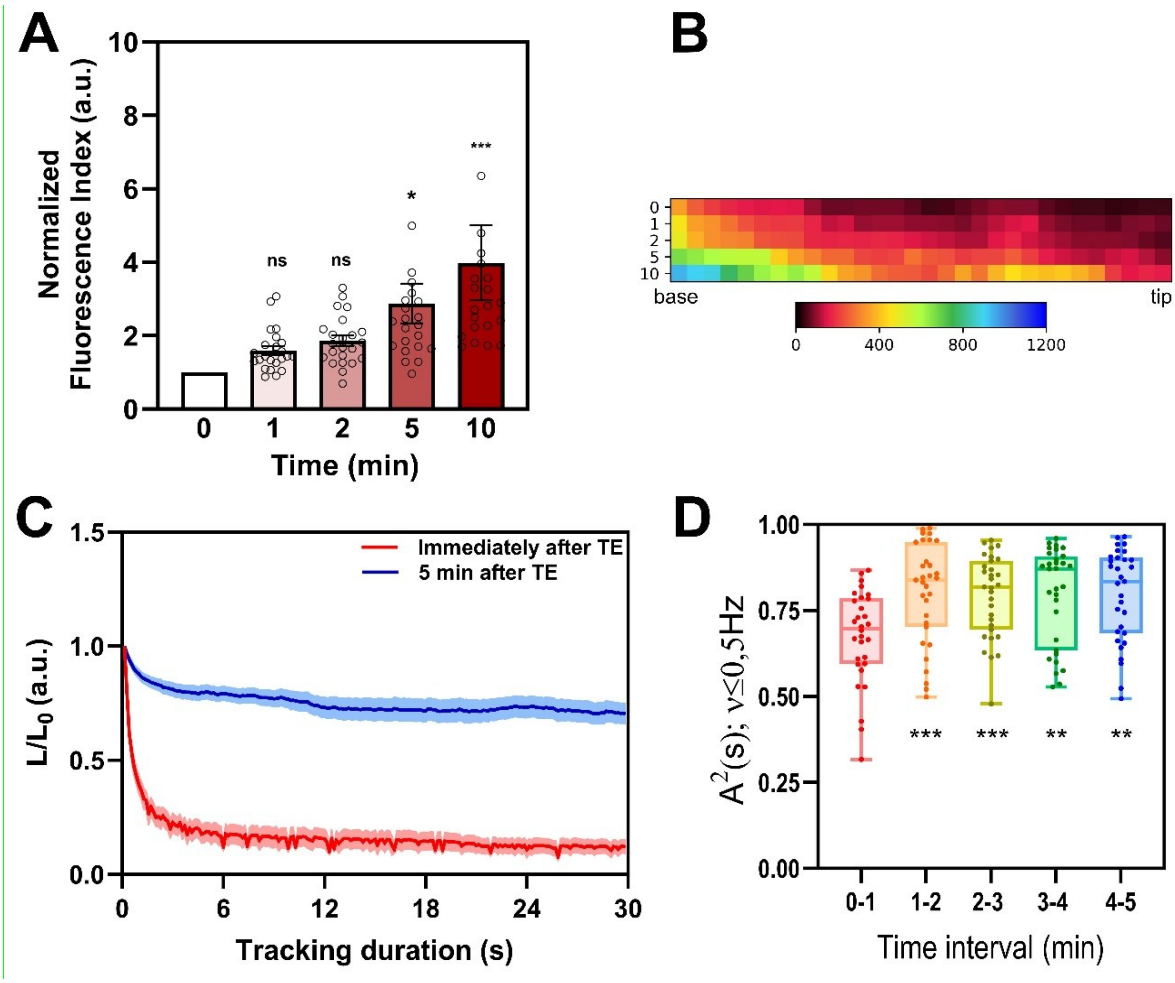


**Fig. S2. NIH3T3 cells cultured in serum-free media – F-actin fluorescence levels, tether recoil and spikes in force.** (A) Average F-actin fluorescence levels measured with Lifeact-mEGFP (normalized to 0 min) for different tethers at each timepoint. Tethers were extracted from NIH3T3 cells cultured in serum-free media (control for MβCD treatment). (B) Plot of tether recoil over time tracking the distance L between the polystyrene beads and cell surfaces (tether extraction sites) for 30 seconds after external point forces were ceased. Conditions: immediately after TE (red curves) and 5 minutes after TE (blue curves). L is normalized to L_0, the initial tether length at the moment forces stopped. Shaded areas represent standard errors; curves show mean values from at least 10 measurements (control for MβCD treatment). (C) Relative contribution of low-frequency force fluctuations (≤ 0.5 Hz), captured by the parameter A^2, across predefined intervals: 0-1 min (red); 1-2 min (orange); 2-3 min (yellow); 3-4 min (green); 4-5 min (blue). Each point represents a measurement within each time interval for NIH3T3 cells cultured in serum-free media (control for MβCD treatment).

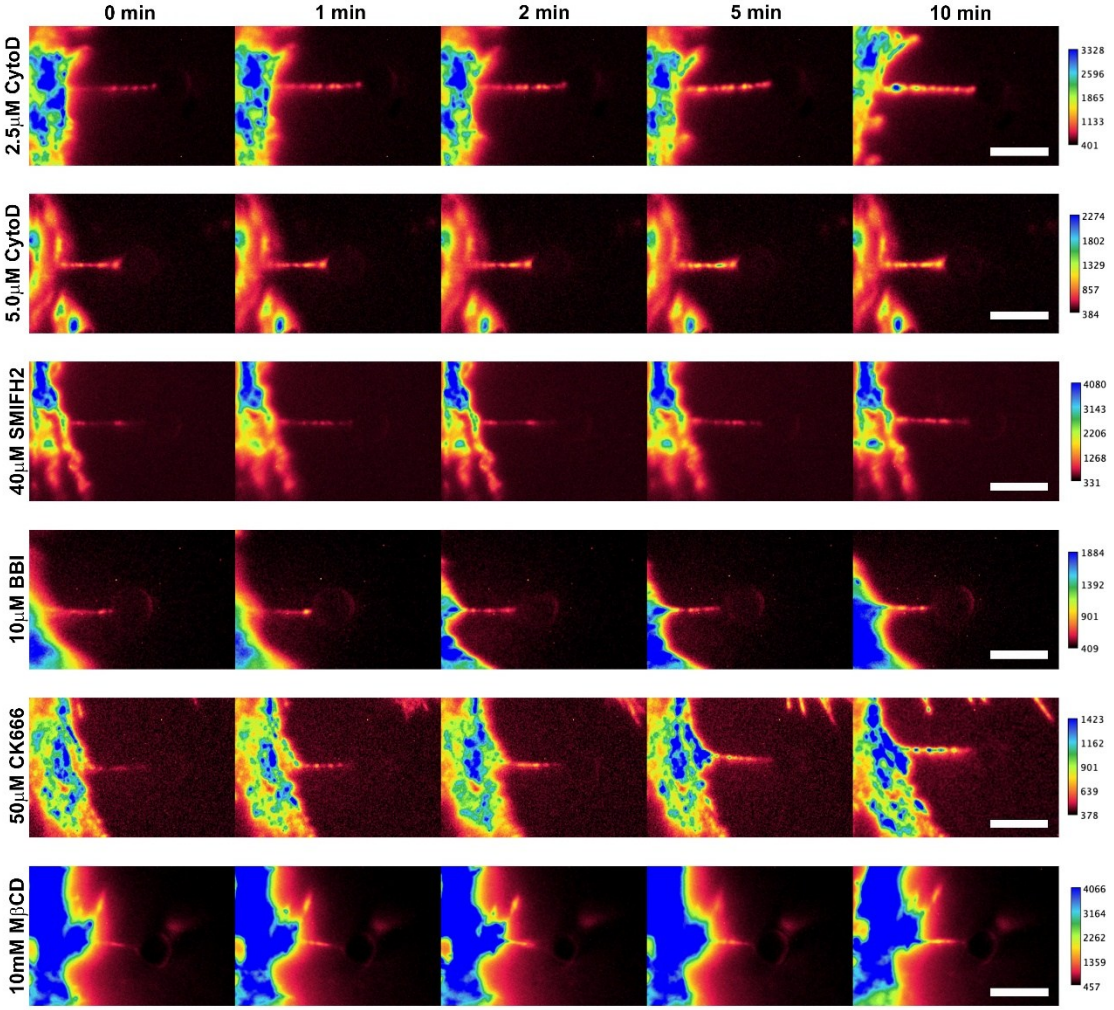


**Fig. S3. Representative images of F-actin distribution within tethers under cytoskeletal perturbations.** NIH3T3 cells expressing Lifeact-mEGFP were subjected to TE, and F-actin distribution was monitored at 0, 1, 2, 5, and 10 minutes under different treatments: (A) 2.5 μM CytoD, (B) 5.0 μM CytoD, (C) 40 μM SMIFH2, (D) 10 μM BBI, (E) 50 μM CK666, and (F) 10 mM MβCD. Each row shows a colormap representation of F-actin intensity along the tether, with the corresponding color scale displayed on the right. Scale bars: 5 μm.

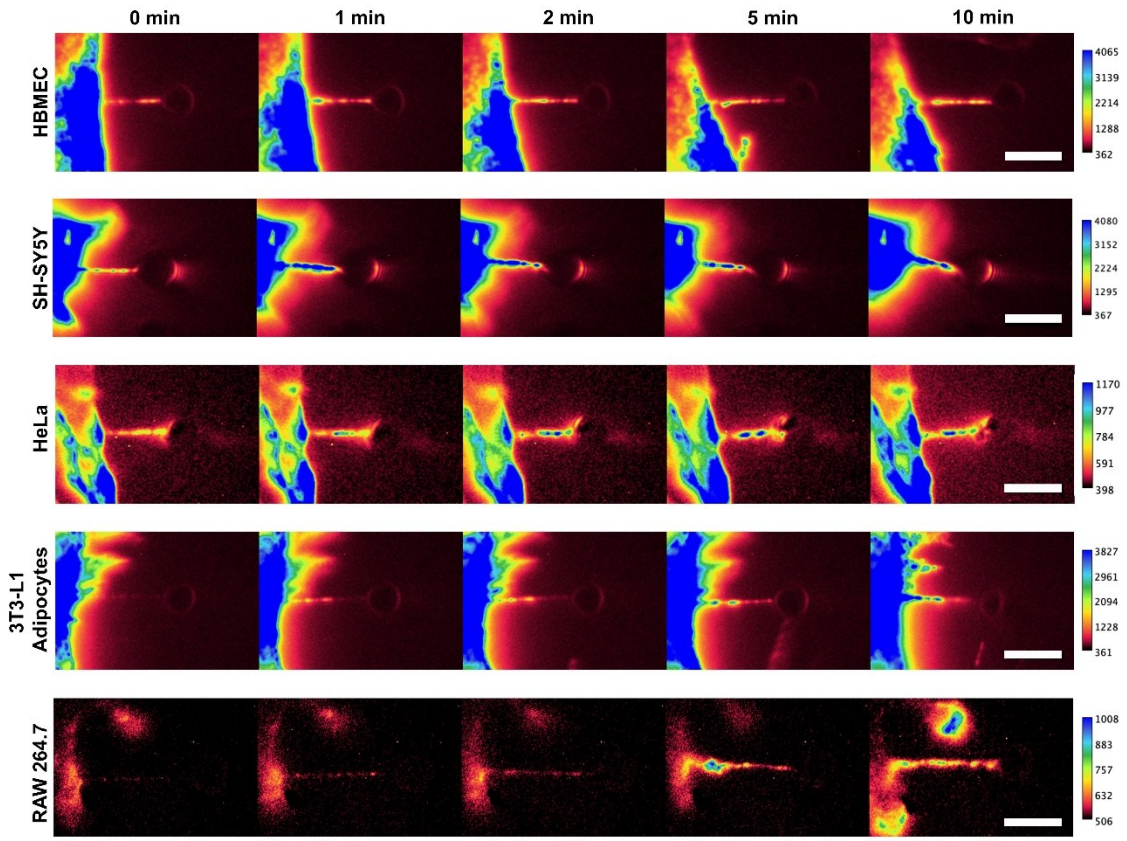


**Fig. S4. Representative images of F-actin distribution within tethers across different cell types.** Cells expressing Lifeact-mEGFP were subjected to TE, and F-actin distribution was monitored at 0, 1, 2, 5, and 10 minutes: (A) HBMEC cells, (B) SH-SY5Y cells, (C) HeLa cells, (D) 3T3-L1 adipocyte-differentiated cells, and (E) RAW264.7 macrophage-like cells. Each row shows a colormap representation of F-actin intensity along the tether, with the corresponding color scale displayed on the right. Scale bars: 5 μm.

**Table S1**

| NIH3T3 serum-free media | $P_1$ | $\tau_1(s)$ | $P_2$ | $\tau_2(s)$ | $P_3$ | $F_0(pN)$ | $\beta_{eq}\ (pN.s.\mu m^{-1})$ |
|---|---|---|---|---|---|---|---|
| Immediately after TE | 0.74 ± 0.02 | 0.68 ± 0.03 | 0.14 ± 0.02 | 5.2 ± 0.8 | 0.12 ± 0.03 | 259 ± 2 | 2.4 ± 0.2 |
| 5 min after TE | 0.152 ± 0.005 | 0.85 ± 0.05 | 0.144 ± 0.004 | 10.1 ± 0.9 | 0.704 ± 0.006 | 23 ± 1 | 12 ± 1 |

**Table S1. Parameters for tether recoil of NIH3T3 cells cultured in serum-free media.**

**Movies S1 to S14**

**Movie S1.**
Immediate force release after membrane tether extraction in a control NIH3T3 cell. A membrane tether was extracted using optical tweezers, and the laser was turned off immediately after TE. The bead rapidly recoiled to the cell surface.

**Movie S2.**
Sustained force application for 5 minutes after tether extraction in a control NIH3T3 cell. A membrane tether was extracted using optical tweezers, and force was maintained for 5 minutes after TE. Upon release, the bead did not recoil to the cell surface, indicating tether increase in mechanical resistance.

**Movie S3.**
Tether force monitoring during 5 minutes in a control NIH3T3 cell. A membrane tether was held for 5 minutes using OT while the tether force was continuously tracked. Spikes in tether force were observed during this period, which can be seen as sudden bead displacements within the trapped bead.

**Movie S4.**
Membrane tether extraction from a Lifeact-mEGFP-transfected NIH3T3 cell. A membrane tether was extracted from a NIH3T3 cell previously transfected with Lifeact-mEGFP. F-actin was present inside the tether with subtle intensity at the initial time points, and increased progressively over time.

**Movie S5.**
Cylindrical protrusion growth from the tether tip. The video shows F-actin extending laterally, forming a cylindrical protrusion from the contact between the tether tip and the bead, with a rate of 30 ± 2 nm/s. Lifeact-mEGFP-transfected NIH3T3 cell.

**Movie S6.**
Nucleation of lamellipodia and fin-like wave protrusions from tethers. The video shows that tethers serve as nucleators for both lamellipodia and fin-like wave protrusions. Lifeact-mEGFP-transfected NIH3T3 cell.

**Movie S7.**
Mechanically formed tethers move along the cell surface, gliding and sliding in response to cell edge dynamics. In a particular event, the protrusion bent, deviating from its original straight form, demonstrating how F-actin-rich tethers can adapt and remodel, mimicking the behavior of the cell surface. Lifeact-mEGFP-transfected NIH3T3 cell.

**Movie S8.**
An external perpendicular force was applied to a pre-formed F-actin-rich tether in a control NIH3T3 cell, resulting in the extraction of a new bifurcated tether.

**Movie S9.**
TNT-like protrusion formation from OT-based tethers. A membrane tether was generated from one cell using optical tweezers and then attached to a neighboring cell, establishing a connection between the two cells.

**Movie S10.**
Stable TNT-like connection. The tether connection remained stable, with the bead returning to the surface of the cell that formed the protrusion, demonstrating the stability of the link between the two cells.

**Movie S11.**
F-actin polymerization and reinforcement within the TNT-like connection. Actin polymerization was observed within the tether connection, reinforcing the structure and maintaining its stability.

**Movie S12.**
Vesicle-like structures passing through the TNT-like bridge. The video shows vesicle-like structures in brightfield moving through the TNT-like bridges formed between two cells, highlighting the dynamic nature of intercellular transport.

**Movie S13.**
Continued vesicle transport through the TNT-like bridge. This movie further demonstrates vesicle-like structures in brightfield passing through the TNT-like bridge, reinforcing the idea that these structures are involved in intercellular communication.

**Movie S14.**
DiI-labeled vesicle-like structures passing through the TNT-like bridge. The video shows vesicle-like structures stained for DiI moving through a mechanically-generated TNT-like bridges formed between two cells.